MLQD: A package for machine learning-based quantum dissipative dynamics

Arif Ullah[1] and Pavlo O. Dral[1]

State Key Laboratory of Physical Chemistry of Solid Surfaces, Fujian Provincial Key Laboratory of Theoretical and Computational Chemistry, Department of Chemistry, and College of Chemistry and Chemical Engineering, Xiamen University, Xiamen 361005, China

(*Electronic mail: ua2024@xmu.edu.cn)

(*Electronic mail: dral@xmu.edu.cn)

(Dated: 1 March 2023)

Machine learning has emerged as a promising paradigm to study the quantum dissipative dynamics of open quantum systems. To facilitate the use of our recently published ML-based approaches for quantum dissipative dynamics, here we present an open-source Python package MLQD (https://github.com/Arif-PhyChem/MLQD), which currently supports the three ML-based quantum dynamics approaches: (1) the recursive dynamics with kernel ridge regression (KRR) method, (2) the non-recursive artificial-intelligence-based quantum dynamics (AIQD) approach and (3) the blazingly fast one-shot trajectory learning (OSTL) approach, where both AIQD and OSTL use the convolutional neural networks (CNN). This paper describes the features of the MLQD package, the technical details, optimization of hyper-parameters, visualization of results, and the demonstration of the MLQD's applicability for two widely studied systems, namely the spin-boson model and the Fenna–Matthews–Olson (FMO) complex. To make MLQD more user-friendly and accessible, we have made it available on the XACS cloud computing platform (https://XACScloud.com) via the interface to the MLatom package (http://MLatom.com).

I. INTRODUCTION

The basic time-dependent Schrödinger equation describes the unitary dynamics of an isolated quantum system. However, isolated quantum systems are an idealistic approximation with many limitations as in real world, systems are always coupled to an environment. Thus, to study quantum systems in reality, it is important to incorporate the effects of environment which gives rise to dephasing and dissipation. Systems with dephasing and dissipation (open quantum systems or quantum dissipative systems) are ubiquitous and can be exploited in environment-assisted quantum transport,[1,2] chemical and biological systems,[3–5] quantum information processing and quantum computing,[6,7] defect tunneling in solids,[8,9] quantum electrodynamics,[10,11] colour centres and Cooper pair boxes,[12,13] quantum optics,[14,15] superconducting junctions,[16] and quarkonium transport in a hot nuclear environment.[17] Exact solution of Schrödinger equation for open quantum systems is a daunting task and in most cases is not feasible because of exponential growth in Hilbert space dimension and a large number of environment degrees of freedom. Thus, many approximations are adopted such as averaging out environment degrees of freedom[18] and classical description of the system and/or environment.[19,20]

In the past three decades, great progress has been made in the development of theoretical approaches for open quantum systems. These approaches include the perturbative Redfield equation,[21] the exact Nakajima–Zwanzig formalism[22,23] and its kernel-based expansions,[24–26] the quantum-classical and fully classical approaches,[20,27–30] Green's function formalism,[31] the transfer tensor method[32] and its extension,[33] the multi-configuration time-dependent Hartree (MCTDH),[34,35] the pseudo-mode approach,[36,37] the reaction coordinate (RC) approach,[38,39] the quantum Monte Carlo (QMC),[40,41] the time-dependent numerical renormalization group (NRG),[42] the density matrix renormalization group (tDMRG),[43] the polaron transformation,[24,44] the time evolving density matrix using the orthogonal polynomial algorithm (TEDOPA),[45,46] the quasiadiabatic propagator path integral (QuAPI),[47,48] the numerical variational method (NVM),[49] the automated compression of environment (ACE) method,[50] the hierarchy equations of motion (HEOM),[51–63] the dissipation equation of motion (DEOM),[64,65] and the stochastic equation of motion (SEOM).[66–80] These methods on their own are successful attempts to solve the complex multibody problem of open quantum systems, however, the prohibitive increase in their computational cost with the system size limits their applicability.

In the past two decades, data proliferation has led to the advent of machine learning (ML) methods. ML has been described as a fourth pillar in Science next to experiment, theory and simulation.[81] Without discussing the broad use of ML, in recent years, ML has seen a surge in the field of quantum dynamics in general and, in particular, quantum dissipative dynamics.[82–107] To be specific, ML has been used to predict molecular configurations in the four-dimensional space,[90] the relaxation dynamics of a two-state system[91–97] the excitation energy transfer in Fenna–Matthews–Olson light-harvesting complex,[98–101] average exciton transfer times and transfer efficiencies,[102] parameters of Hamiltonian,[103] evolution of the proton density in a potential well[104] and vibronic Hamiltonians as a direct function of time.[105] Machine learning has also been extended to Meyer–Miller mapping based symmetrical quasi-classical[106] and fewest-switches surface hopping dynamics.[107]

The rapid development of new ML methods for quantum dissipative dynamics led to so-far not well-organized and scattered software implementations. In this article, we present an open-source software package MLQD, version 1, which provides a framework for ML-based quantum dissipative dynamics implementations. MLQD is incorporated with kernel ridge regression (KRR) and convolutional neural networks (CNN) models and a user can train and predict dynamics following both recursive and non-recursive approaches. We follow our recently published recursive KRR-based approach on the relaxation dynamics of the spin-boson model[91,92] and non-recursive CNN-based AIQD and OSTL approaches.[98,99] MLQD also supports hyperparameter optimization using MLATOM's grid search functionality[108–110] for KRR and Bayesian methods with Tree-structured Parzen Estimator (TPE)[111] for CNN models via the HYPEROPT package.[112] In addition, we also incorporate the visualization of results by auto-plotting. MLQD has also been interfaced with the MLATOM package[108–110] which allows the user to run MLQD on the XACS cloud computing platform.[113]

In the following, we provide an overview of the MLQD package, the theory of implemented approaches, technical details, optimization of hyperparameters, visualization of results, and the demonstration of MLQD's applicability for two widely studied systems, namely the spin-boson model and the Fenna–Matthews–Olson (FMO) complex.

II. MLQD PACKAGE OVERVIEW

MLQD package is written in Python language and provides the implementation of our recently proposed ML-based approaches for quantum dissipative dynamics.[91,98,99] This section lays out the concise documentation of theory, code design, use and implementation. Coming to the code design, we provide a simplified flowchart of MLQD architecture in Fig. 1.

A. ML-based quantum dynamics approaches

ML-based quantum dynamics approaches can be divided into two main categories: recursive approaches and non-recursive.

1. *Recursive approaches*

In recursive approaches, the future dynamics depends on its past dynamics which in nature is the same as in traditional quantum dynamics approaches. In these approaches, an initial shot-time dynamics of time-length t_m is used as an input to predict system dynamics at the next time step t_{m+1}, i.e., $\tilde{\rho}_s(t_{m+1}) = f_{ML}(\tilde{\rho}_s(t_0), \tilde{\rho}_s(t_2), \ldots, \tilde{\rho}_s(t_m))$ where $\tilde{\rho}_s(t)$ is the reduced density matrix (RDM) of the system at time t (see Section III) and f_{ML} is ML function. To incorporate the recursiveness of the dynamics, in the next step, the predicted dynamics at t_{m+1} is appended to the end of the input vector while the value at the start of the input vector is dropped which leads to a new input of the same size as the old input. The new input is used to predict system dynamics at the next time step t_{m+2}, i.e., $\tilde{\rho}_s(t_{m+2}) = f_{ML}(\tilde{\rho}_s(t_1), \tilde{\rho}_s(t_2), \ldots, \tilde{\rho}_s(t_{m+1}))$. To predict system dynamics at t_{m+3}, the predicted dynamics at t_{m+2} is included with the drop of time step at the first end and this process continues till the last time step. In Fig. 2, we have elaborated on the transformation of the training trajectories into the training data for machine learning. Following Ref. 91, in MLQD, the recursive approach is adopted only for the KRR model and we will refer to this approach as the KRR approach (see Subsection II B 1).

2. *Non-recursive approaches*

Recursive approaches have the downside that they should be run sequentially, one step at a time, which is intrinsically computationally costly. An additional downside is the potential for error accumulation at each time step. To develop approaches that are free of these downsides, we have recently proposed two non-recursive approaches AIQD (artificial intelligence-based quantum dynamics[98]) and OSTL (one-shot trajectory learning[99]). Non-recursive approaches are based on neural networks, details are given in Subsection II B 2. In the following, we briefly describe both approaches.

a. AIQD approach. In the AIQD approach,[98] the dynamics is predicted as a continuous function of time, i.e., dynamics property (system's state) can be predicted at an arbitrary time without step-wise dynamics propagation. Unlike recursive approaches, AIQD does not need to use short-time dynamics as an input. Input, in addition to time, includes simulation parameters such as temperature T, characteristic frequency γ and system-bath coupling strength λ. The dynamics corresponding to these parameters is used as a target vector (for training) and predicted by the model when used for inference. In addition, as all time steps are independent of each other, parallel computation of all time steps is possible. Fig. 3 shows data preparation for the AIQD approach where each trajectory transforms into the training points equal to the number of time steps. We also note that to make predictions in asymptotic limit and cover different time regions with similar accuracy, the time input is mapped into a multi-dimensional vector after normalization with the logistic function.

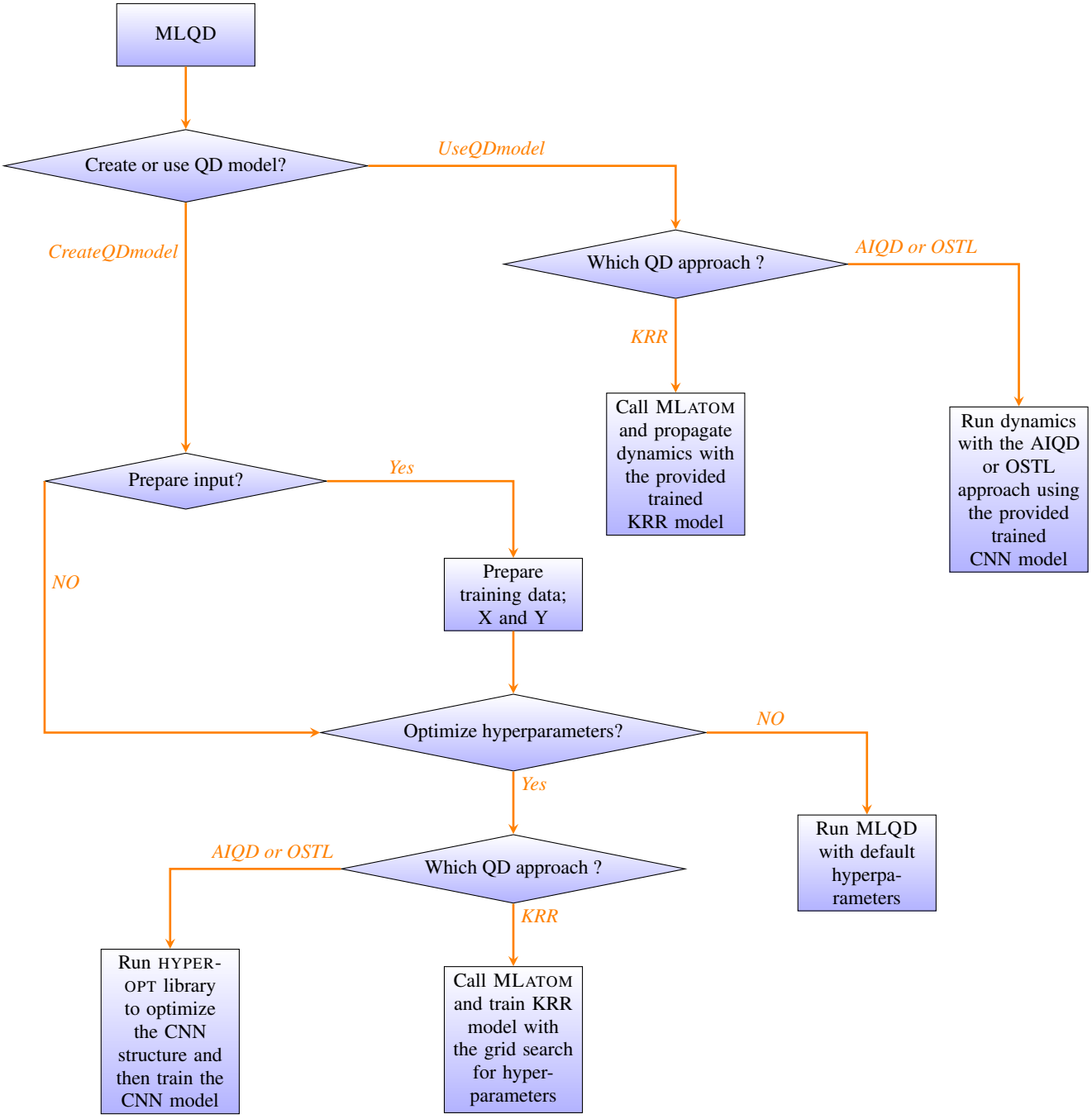

FIG. 1. A simplified flowchart of the MLQD package with two main features, *createQDmodel* which trains a QD model and *useQDmodel* which uses the already trained QD model for dynamics propagation. MLQD has also the feature of preparing the training data X and Y considering the training trajectories are given in the same format as in our QD3SET-1.[114] MLQD can also optimize the hyperparameters using the grid search for KRR model (utilizing MLATOM[108–110] in the backend) and HYPEROPT library[112] in the case of AIQD and OSTL approaches.

b. OSTL approach. Similar to the AIQD approach, in the OSTL approach[99] dynamics property (system's state) can be predicted without step-wise dynamics propagation. However, in contrast to the AIQD, OSTL predicts entire trajectory in one shot for a discretized set of time steps. OSTL also includes the simulation parameters (i.e., λ, γ, T) as an input, while time is not included. As shown in Fig. 4, in the OSTL approach, each trajectory transforms into a single training point thus significantly reducing the cost of training. The full-time dynamics is predicted using the multi-output feature which obviates invoking the entire ML structure for each time step, thus leading to a significant speed up in dynamics prediction too.

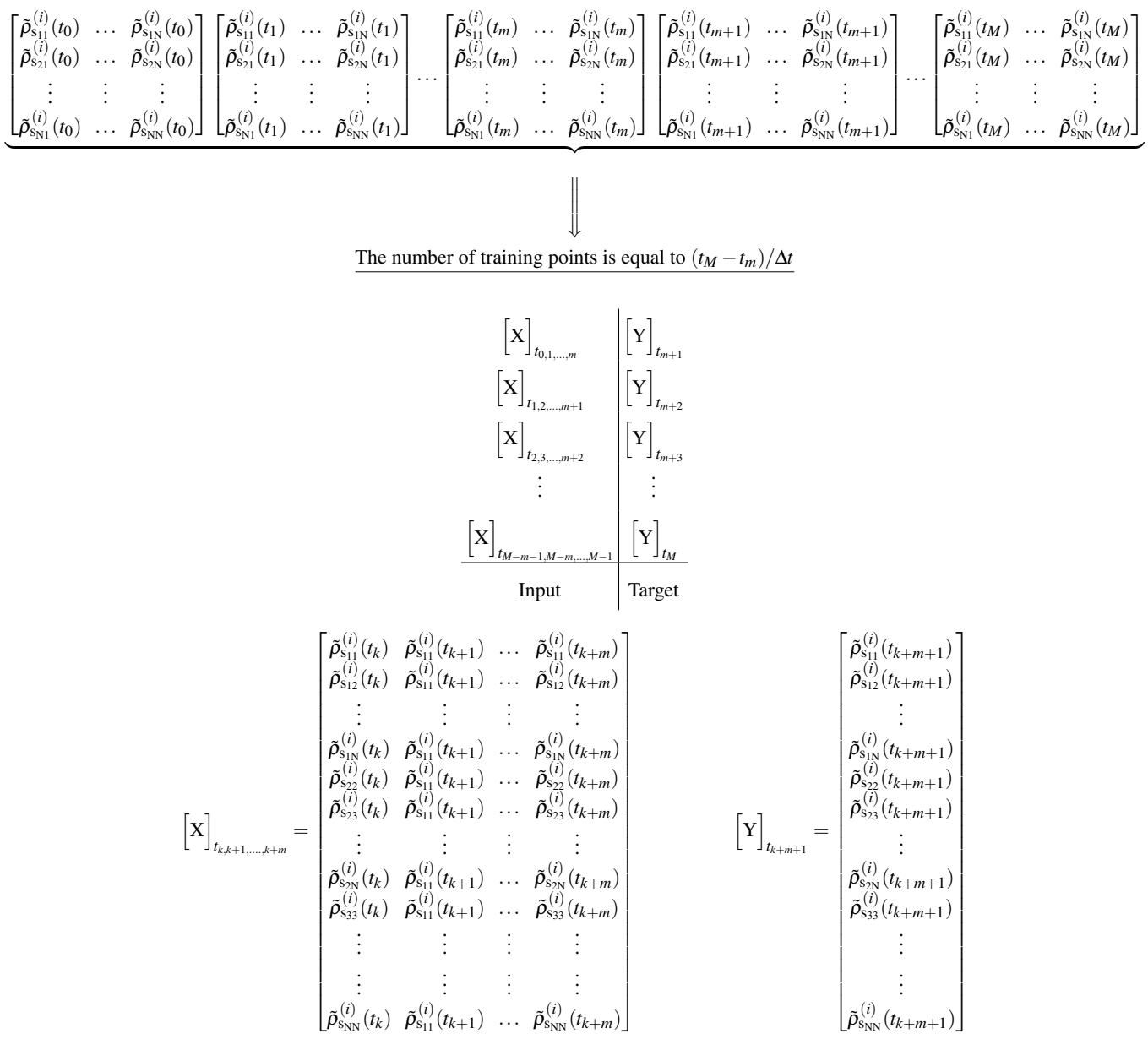

FIG. 2. Transformation of the quantum dynamics trajectories into the training data for the recursive approach on an example of the RDM terms.

B. Machine learning models

1. *Kernel ridge regression*

In kernel ridge regression (KRR), for a given input vector $\mathbf{r}$, a function $f(\mathbf{r})$ is approximated with the following expansion[108,115]

$$f(\mathbf{r}) = \sum_{i}^{N_{tr}} \eta_i \mathrm{K}(\mathbf{r}, \mathbf{r}_i), \tag{1}$$

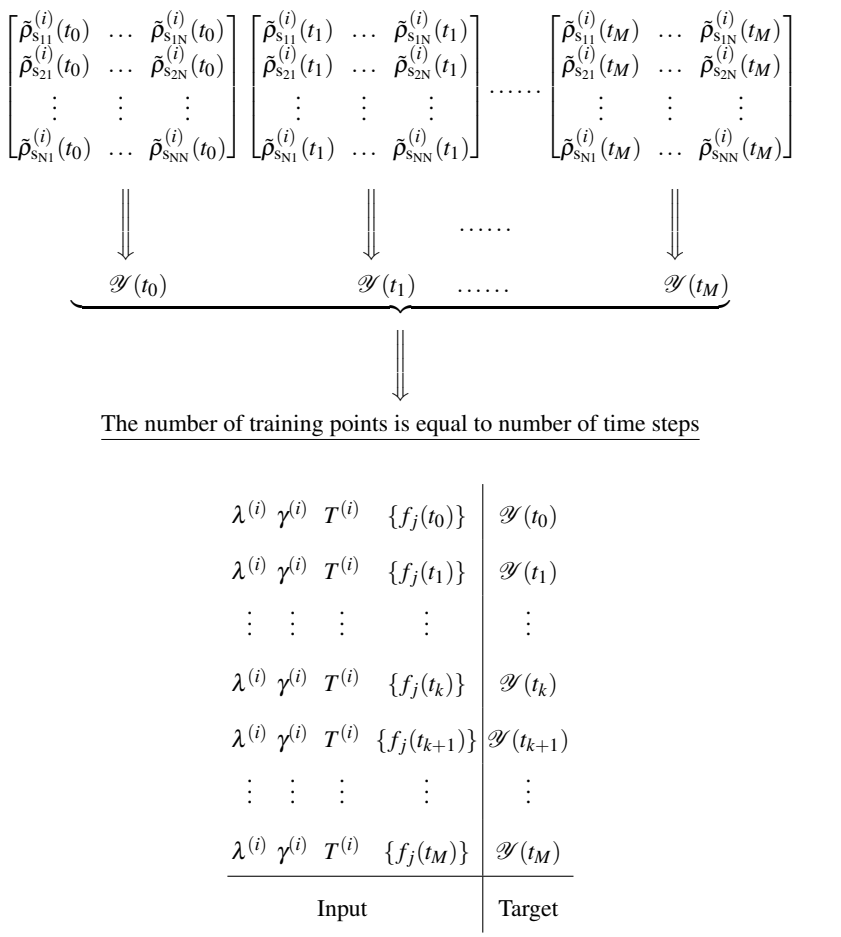

FIG. 3. Transformation of the ith trajectory of RDM $\tilde{\rho}^{(i)}_{\rm s}(t)$ in the AIQD approach. The $\tilde{\rho}^{(i)}_{\rm s}(t)$ at each time step transforms into a vector $\mathscr{Y}(t)$ with dimension M = number of sites + (2 $\times$ number of the upper off-diagonal terms). As in RDM $\tilde{\rho}_{\rm s_{nm}}(t)=\tilde{\rho}^{*}_{\rm s_{mn}}(t)\,(n\neq m)$, only the upper off-diagonal terms are learned. In addition, the real and imaginary parts of each off-diagonal term are separated. Simulation parameters $\lambda^{(i)}$, $\gamma^{(i)}$ and $T^{(i)}$ are the reorganization energy, characteristic frequency, and temperature of the ith trajectory in their respective order. The $\{f(t)\}$ is a set of logistic functions normalizing the dimension of time, i.e., $f_j(t)=a/\left(1+b\exp\left(-(t+c_j)/d\right)\right)$ where a, b, d are fixed constants while $c_j=5j-1$ having j as a natural number, i.e., $j\in\{0,1,2,3,\ldots\ldots\}$.

where N_{tr} is the number of training points, $\eta=\{\eta_i\}$ is a vector of regression coefficients and $\mathrm{K}(\mathbf{r},\mathbf{r}_i)$ is a kernel function measuring the similarity between two vectors $\mathbf{r}$ and $\mathbf{r}_i$. The very common kernel is the Gaussian kernel[108,116]

$$\mathrm{K}(\mathbf{r},\mathbf{r}_i)=\exp\left(-\frac{\|\mathbf{r}-\mathbf{r}_i\|_2^2}{2\sigma^2}\right), \tag{2}$$

where σ is a hyperparameter defining the length scale. It is worth emphasising that many other kernel functions $\mathrm{K}(\mathbf{r},\mathbf{r}_i)$ such as Matérn and exponential kernels[117,118] can also be used, however, based on our previous studies,[91,92] these kernels do not outperform the Gaussian kernel, thus in MLQD, we only use the Gaussian kernel.

To find the regression coefficients η in Eq. (1), MLQD uses MLATOM package[108–110] in the backend and solves the following equation

$$(\mathbf{K}+\lambda\mathbf{I})\,\eta=\mathbf{y}, \tag{3}$$

where $\mathbf{K}$ is the kernel matrix, $\mathbf{I}$ is the identity matrix, $\mathbf{y}$ is the vector of target values, and λ represents a non-negative regularization hyperparameter.

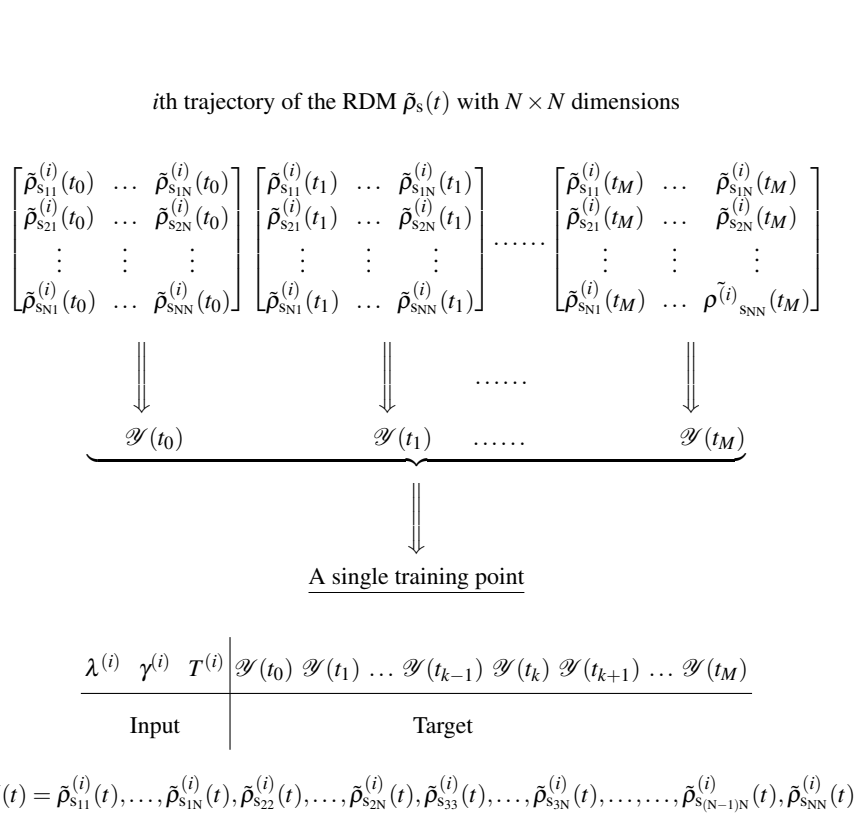

FIG. 4. Transformation of the ith trajectory of RDM $\tilde{\rho}_s^{(i)}(t)$ in the OSTL approach. The $\tilde{\rho}_s^{(i)}(t)$ at each time step transforms into a vector $\mathscr{Y}(t)$ with dimension M = number of sites + (2 × number of the upper off-diagonal terms). As in RMD $\tilde{\rho}_{s_{nm}}(t) = \tilde{\rho}^*_{s_{mn}}(t)\,(n \neq m)$, only the upper off-diagonal terms are learned. In addition, the real and imaginary parts of each off-diagonal term are separated. Simulation parameters $\lambda^{(i)}$, $\gamma^{(i)}$ and $T^{(i)}$ are the reorganization energy, characteristic frequency, and temperature of the ith trajectory in their respective order.

2. *Neural networks*

Carefully-constructed neural networks (NN) models, consisting of neurons organized in layers, can be considered as universal approximators of any continuous function.[119–121] There is a large group of NN models that can be used to learn and predict quantum dynamics,[92] however here we will restrict ourselves to the convolutional neural network (CNN) model as it is the only NN model implemented in the MLQD package. As shown in Fig. 5, the CNN model in MLQD package comprises of an input layer, two or three convolutional layers, a maximum pooling layer, a flatten layer, two or three dense layers and an output layer. In CNN, convolutional layers extract the features such as time dependence, the maximum pooling layer decreases the size of the feature map, the flatten layer transforms the output from the maximum pooling layer into one-dimensional vector and then we have the dense layers which are the common feed-forward neural networks.

C. Optimization of hyperparameters

In the MLQD package, we provide a set of default values for hyperparameters, however, the hyperparameter optimization is also possible. In the case of KRR approach, MLQD uses MLATOM's grid search functionality and optimizes its both hyperparameters σ and λ. In the case of AIQD and OSTL approaches, MLQD uses the HYPEROPT library[112] for the optimization of CNN structure. HYPEROPT uses Bayesian optimization with the parallel infrastructure for a fast search of best hyperparameters in a defined multidimensional space. We optimize the number of filters, kernels size, the number of neurons, learning rate and the number of batches in a predefined multidimensional space. The number of hidden convolutional layers and hidden dense layers are optimized between two numbers, i.e., $\{2, 3\}$.

D. Plotting

For a better understanding of any approach, visualization of results is necessary and in many cases such as cloud computing, auto-plotting provides complete mouse-click computing. We incorporate this functionality in MLQD, where the predicted

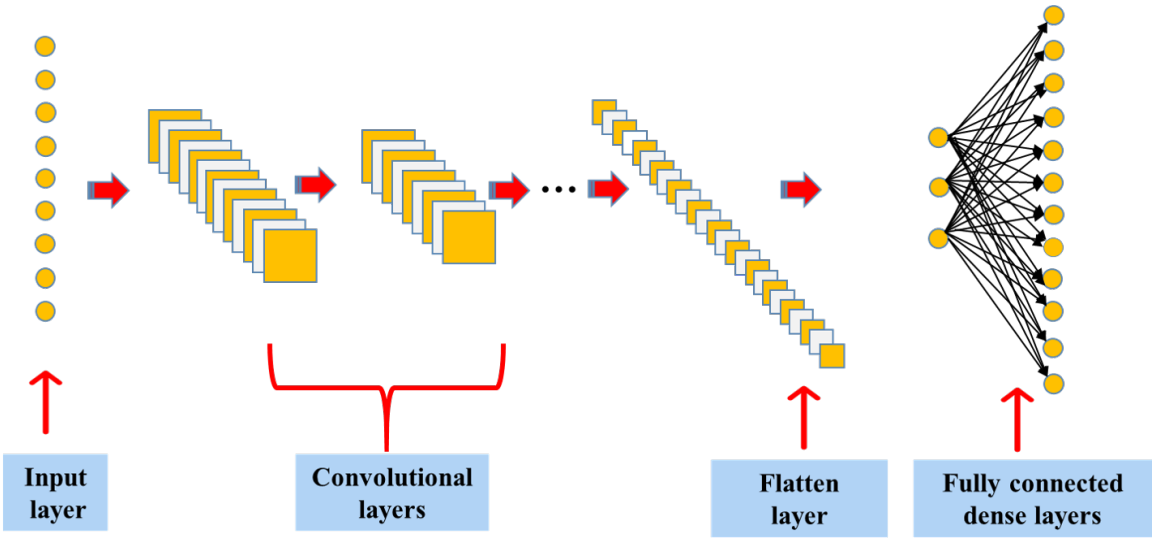

FIG. 5. A flowchart of CNN model in MLQD which consists of an input layer, convolutional layers, a maximum pooling layer (not shown), a flatten layer, dense layers and an output layer.

dynamics is plotted against the reference trajectory providing a clear visualization of the predicted dynamics.

III. APPLICATIONS

In this section, we present two case studies to highlight the applications of the MLQD package. We consider the two widely studied systems, namely the spin-boson model and the Fenna–Matthews–Olson (FMO) complex.

Before that, we briefly overview the general theory behind open quantum systems. A quantum system coupled to its outside environment (bath) is regarded as an open quantum system with the dynamics governed by the following Hamiltonian

$$\mathbf{H} = \mathbf{H}_{\mathrm{s}} + \mathbf{H}_{\mathrm{b}} + \mathbf{H}_{\mathrm{sb}}, \tag{4}$$

where $\mathbf{H}_{\mathrm{s}}$ and $\mathbf{H}_{\mathrm{b}}$ represent the Hamiltonian for the system and the outside environment (bath), respectively. The last term $\mathbf{H}_{\mathrm{sb}}$ incorporates the interaction between the system and the environment. To propagate quantum dynamics, Liouville–von Neumann equation can be employed

$$\dot{\rho}(t) = -i[\mathbf{H}, \rho(t)], \tag{5}$$

where $\rho(t)$ is the density matrix at time t and $\hbar$ is set to 1. In system-bath approaches,[51,52,64,70] calculations are usually simplified by considering system and environment uncorrelated at $t = 0$, i.e., $\rho(0) = \rho_{\mathrm{s}}\rho_{\mathrm{b}}$ where ρ_{s} is the density matrix of the system and ρ_{b} denotes density matrix of the environment. As we are interested only in the system, we can take a partial trace over environment degrees of freedom

$$\tilde{\rho}_{\mathrm{s}} = \mathbf{Tr}_{\mathrm{b}}\left[\mathbf{U}(t,0)\rho(0)\mathbf{U}^{\dagger}(t,0)\right], \tag{6}$$

where $\tilde{\rho}_{\mathrm{s}}$ is the density matrix of the reduced system (reduced density matrix (RDM)) and $\mathbf{U}(t,0)$ $\left(\mathbf{U}^{\dagger}(t,0)\right)$ is the propagation operator forward (backward) in time and $\mathbf{Tr}_{\mathrm{b}}$ is the partial trace over environment degrees of freedom. In reality, the term *open quantum system* is applicable to most of the systems, however, because of the curse of dimensionality, not all of them are easy to be theoretically handled. In the following, we present a brief theory of two broadly studied pedagogical systems, the two-states spin-boson model and the FMO complex.

A. Case study 1: Relaxation dynamics of spin-boson model

As a first case study, we consider the relaxation dynamics of excited state $|e\rangle$ in spin-boson model. The spin-boson model is a two-state system coupled with an environment of an infinite number of non-interacting harmonic oscillators. The Hamiltonian

of the composite system (two-states system + environment) is expressed as

$$\mathbf{H} = \varepsilon\left(|e\rangle\langle e| - |g\rangle\langle g|\right) + \Delta\left(|e\rangle\langle g| + |g\rangle\langle e|\right) + \sum_{k=1}\omega_k \mathbf{b}_k^\dagger \mathbf{b}_k + \left(|e\rangle\langle e| - |g\rangle\langle g|\right)\sum_{k=1} c_k\left(\mathbf{b}^\dagger + \mathbf{b}_k\right), \tag{7}$$

where $|e\rangle$ and $|g\rangle$ denote the two states of the system, ε is the energy difference between the two states and Δ is the tunneling splitting. The $\mathbf{b}_k^\dagger(\mathbf{b}_k)$ denotes the creation (annihilation) operator in the environment Hilbert space and ω_k is the frequency corresponding to k mode. The last term in Eq. (7) incorporates the interaction between the system and environment with c_k as the coupling strength between the system's operator and k environment mode. The effects of the environment on system dynamics are described by the spectral density of the environment

$$J(\omega) = \sum_k \alpha_k \delta(\omega - \omega_k), \tag{8}$$

where $\alpha_k = \frac{\pi}{2}\frac{c_k^2}{m_k\omega_k}$. Here we adopt the Ohmic spectral density function with the Drude–Lorentz cut-off[122]

$$J(\omega) = 2\lambda\frac{\gamma\omega}{\omega^2+\gamma^2}, \tag{9}$$

where λ is the reorganization energy and γ is the characteristic frequency or the inverse of environment relaxation time, i.e., $\gamma = 1/\tau$.

For our example, we use the spin-boson data set from our recently published QD3SET-1 database.[114] The mentioned data set consists of 1000 trajectories generated for each possible combination of the following parameters; $\tilde{\varepsilon} = \varepsilon/\Delta = \{0,1\}$, $\tilde{\lambda} = \lambda/\Delta = \{0.1, 0.2, 0.3, 0.4, 0.5, 0.6, 0.7, 0.8, 0.9, 1.0\}$, $\tilde{\gamma} = \gamma/\Delta = \{1,2,3,4,5,6,7,8,9,10\}$, and $\tilde{\beta} = \beta\Delta = \{0.1, 0.25, 0.5, 0.75, 1\}$, where the tunneling matrix element Δ is set as an energy unit. Data is generated with the HEOM method implemented in the QuTiP software package[123] and each trajectory is propagated up to $t\Delta = 20$ with the time step $dt\Delta = 0.05$.

In this case study, we use all three available approaches (i.e., KRR, AIQD and OSTL) to predict the relaxation dynamics in the two possible cases, namely the symmetric case $\tilde{\varepsilon} = 0$ and the asymmetric case $\tilde{\varepsilon} = 1.0$. Before training, we divide the spin-boson data set into the training set (400 trajectories for each case) and the test set (100 trajectories for each case). The division is based on farthest-point sampling which selects the most distant points in a three-dimensional Euclidean space[98] $(\tilde{\lambda}, \tilde{\gamma}, \tilde{\beta})$, thus efficiently covering the parameter space in comparison to random sampling.[108] Keeping in mind the high computational cost of KRR, we sample the data for training with comparatively larger time step $dt\Delta = 0.1$.

For KRR, a short-time trajectory of $t_m\Delta = 4.0$ is used as an input and following the algorithm described in Fig. 2,[91] we transform the trajectories beyond $t_m\Delta = 4.0$ into target values. We train separate KRR models for each diagonal element of the RDM. As $\tilde{\rho}_{s_{12}} = \tilde{\rho}^*_{s_{21}}$, we learn only the upper off-diagonal term where we train a separate KRR model for real and imaginary parts. After training, we provide a reference short-time trajectory of time-length $t_m\Delta = 4.0$ to initiate recursive propagation with the trained KRR model (the recursive propagation is beyond this short-time trajectory dynamics). In Fig. 6(A), we show population and coherence for symmetric case $\tilde{\varepsilon} = 0$ while results for asymmetric case $\tilde{\varepsilon} = 1$ are shown in Fig. S1(A).

In the case of AIQD and OSTL approaches, we prepare training data following Figs. 3 and 4 in their respective order. In both approaches, we use $\tilde{\gamma}_{\max} = 10.0$ for $\tilde{\gamma}$ and 1.0 for the remaining simulation parameters as normalization factors. To normalize the dimension of time, in AIQD we use a set of 10 logistic functions, i.e., $f_j(t) = a/\left(1 + b\exp\left(-(t+c_j)/d\right)\right)$ where $j = 0, 1, 2, \ldots, 9$. We set $a = 1.0$, $b = 15.0$, $d = 1.0$ and $c = 5j - 1$. In List. 1, we show an example of MLQD input for creating (training) a CNN model following the OSTL approach. After training, by providing the trained AIQD model, values of the simulation parameters and time, MLQD predicts the corresponding RDM $\tilde{\rho}_s$. In the OSTL approach, the RDM $\tilde{\rho}_s$ is predicted for the whole time range, i.e., $t_m\Delta = 0, \ldots, \ldots t_m\Delta = 20$. In Figs. 6(B) and (C), we show the time evolution of RDM's diagonal (population) and off-diagonal terms (coherence) for a set of test parameters. Results for the asymmetric case $\tilde{\varepsilon} = 1$ are given in Figs. S1(B) and (C).

```
import os
import sys

MLQD_PATH='path/to/MLQD/package'
if MLQD_PATH not in sys.path:
    sys.path.append(MLQD_PATH)

from evolution import quant_dyn
param={
       'n_states': 2,
       'QDmodel': 'createQDmodel',
       'QDmodelType': 'OSTL',
```

```
        'prepInput' : 'True',
        'XfileIn': 'x_data',
        'YfileIn': 'y_data',
        'energyNorm': 1.0,
        'DeltaNorm': 1.0,
        'gammaNorm': 10.0,
        'lambNorm': 1.0,
        'tempNorm': 1.0,
        'systemType': 'SB',
        'hyperParam': 'True',
        'patience': 100,
        'OptEpochs': 100,
        'TrEpochs': 1000,
        'max_evals': 50,
        'dataPath': '/path/to/training_trajectories',
        'QDmodelOut': 'OSTL_CNN_SB_model'
        }
quant_dyn(**param)
```

Listing 1. An example of MLQD input for creating (training) a CNN model following OSTL approach.

B. Case study 2: Excitation energy transfer in FMO complex with AIQD approach

In our second case study, we consider excitation energy transfer in the FMO complex which is described by the Frenkel exciton model with the following Hamiltonian[124]

$$\begin{aligned} \mathrm{H} = &\sum_{n=1}^{N} |n\rangle \varepsilon_n \langle n| + \sum_{n,m=1,n\neq m}^{N} |n\rangle J_{nm} \langle m| + \sum_{n=1}^{N}\sum_{k=1} \left(\frac{1}{2}\mathrm{P}_{k,n}^2 + \frac{1}{2}\omega_{k,n}^2 \mathrm{Q}_{k,n}^2 \right) \\ &- \sum_{n=1}^{N}\sum_{k=1} |n\rangle c_{k,n} \mathrm{Q}_{k,n} \langle n| + \sum_{n=1}^{N} |n\rangle \lambda_n \langle n| \,, \end{aligned} \tag{10}$$

where N is the number of sites (bacteriochlorophyll molecules), ε_n is the energy of the nth site and J_{nm} denotes the inter-site coupling between sites n and m. The third term in Eq. (10) describes the environmental part with $\mathrm{P}_{k,n}$ as conjugate momentum, $\mathrm{Q}_{k,n}$ as coordinate and $\omega_{k,n}$ as a frequency of the corresponding environment mode k. λ_n is the reorganization energy associated with site n and the strength of the coupling between environment mode k and site n is represented by $c_{k,n}$. In the case of FMO complex, we assume that all sites have the same spectral density as described by Eq. (9).

In our example, we take the 8-site FMO complex where three sites (1, 6 and 8) have an equal probability of getting initially excited while the reaction center is in the vicinity of sites 3 and 4. For training, we use the FMO-IV data set from the QD3SET-1 database[114] generated for the following Hamiltonian[125,126]

$$H_s = \begin{pmatrix} 310 & -80.3 & 3.5 & -4.0 & 4.5 & -10.2 & -4.9 & 21.0 \\ -80.3 & 230 & 23.5 & 6.7 & 0.5 & 7.5 & 1.5 & 3.3 \\ 3.5 & 23.5 & 0 & -49.8 & -1.5 & -6.5 & 1.2 & 0.7 \\ -4.0 & 6.7 & -49.8 & 180 & 63.4 & -13.3 & -42.2 & -1.2 \\ 4.5 & 0.5 & -1.5 & 63.4 & 450 & 55.8 & 4.7 & 2.8 \\ -10.2 & 7.5 & -6.5 & -13.3 & 55.8 & 320 & 33.0 & -7.3 \\ -4.9 & 1.5 & 1.2 & -42.2 & 4.7 & 33.0 & 270 & -8.7 \\ 21.0 & 3.3 & 0.7 & -1.2 & 2.8 & -7.3 & -8.7 & 505 \end{pmatrix}, \tag{11}$$

with the diagonal offset of 12195 cm^{-1}. In the considered data set, exciton dynamics is propagated for the most distant 500 combinations of the following parameters: $\lambda = \{10, 40, 70, \ldots, 520\}$ cm^{-1}, $\gamma = \{25, 50, 75, \ldots, 500\}$ cm^{-1}, and T = {30, 50, 70, …, 510} K. The chosen 500 trajectories are propagated for each possible case of initial excitation (i.e., on sites 1, 6 and 8) with time length $t = 50$ ps and time step $dt = 5$ fs. Calculations are performed with the local thermalizing Lindblad master equation (LTLME) approach,[127,128] implemented in the QUANTUM_HEOM package.[129] In order to make it compatible with the Hamiltonians with larger dimensions, the package is modified locally.

We choose our training trajectories (400 for each case of initial excitation) and test trajectories (100 for each case of initial excitation) based on farthest-point sampling. In this case study, we consider only the AIQD and OSTL approaches as training the KRR model (in the current implementation) is not feasible because of its high computational cost. In both approaches (AIQD

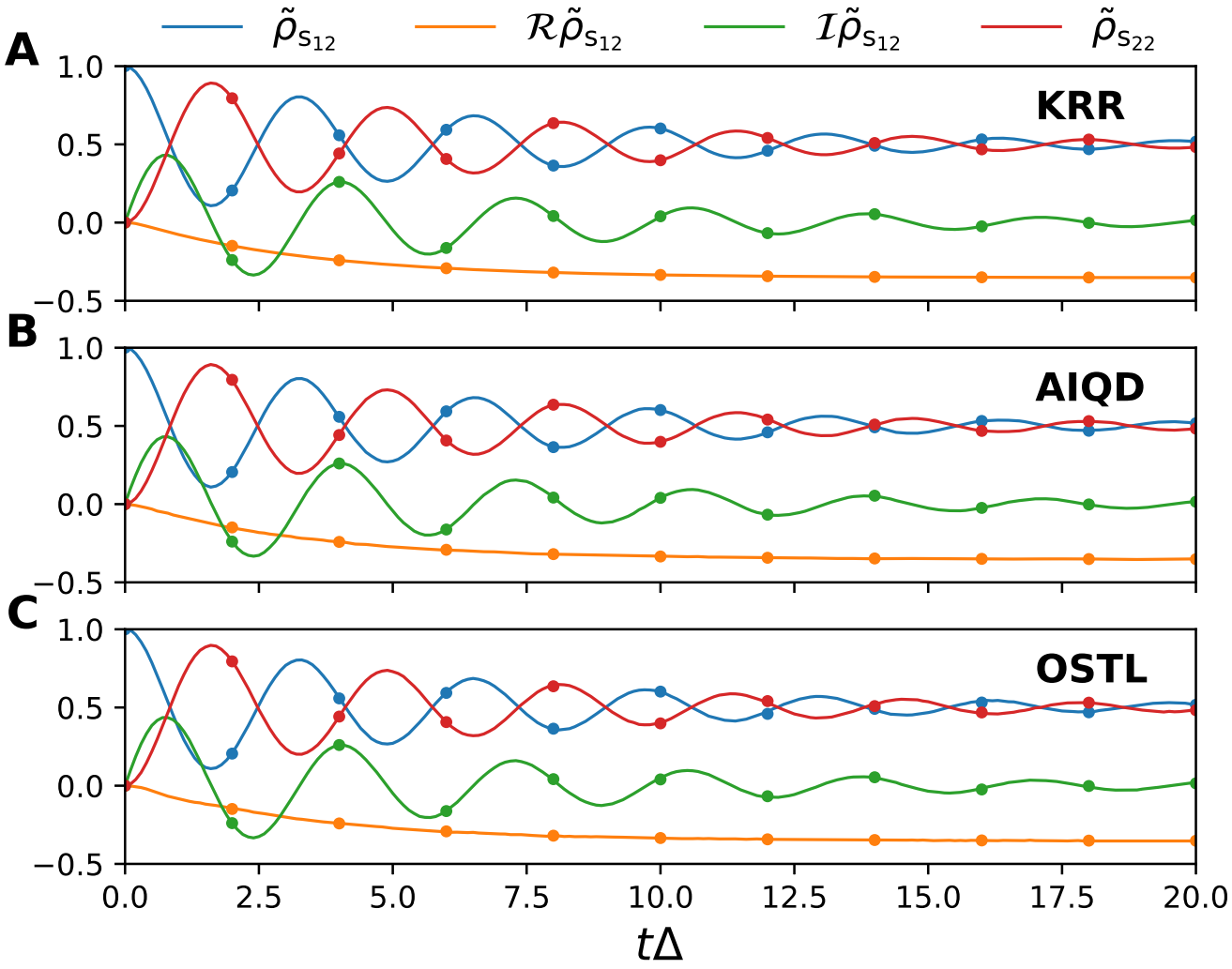

FIG. 6. The time evolution of the diagonal (population) and off-diagonal terms (coherence) of the reduced density matrix (RDM) $\tilde{\rho}_s$ predicted with the recursive (KRR) and non-recursive (AIQD and OSTL) approaches. The calligraphic R and I denote the real and imaginary parts of the off-diagonal terms, respectively. Results are shown for the symmetric spin-boson model ($\tilde{\varepsilon} = 0.0$) with the following set of unseen parameters: $\tilde{\gamma} = 10.0$, $\tilde{\lambda} = 0.3$, $\tilde{\beta} = 1.0$. The predicted results are compared to the reference HEOM method (dots).

and OSTL), we use $\lambda_{\max} = 520$, $\gamma_{\max} = 500$ and $T_{\max} = 510$ as normalizing factors for the corresponding simulation parameters (i.e., λ, γ and T). In AIQD, we use the same number of logistic functions and the same constants as was adopted for the spin-boson case. After training, we pass a set of unseen simulation parameters and MLQD predicts the corresponding dynamics using the trained CNN models. In the described order, Figs 7 and 8 show the excitation energy transfer (diagonal terms of RDM) and the time evolution of coherent terms (off-diagonal terms of RDM) for a test trajectory. The presented results are with the initial excitation on site 1 and results for the initial excitation on sites 6 and 8 are given in Figs. S2-5. In List. 2, we show an example of the MLQD input for predicting exciton dynamics in the FMO complex using the OSTL approach.

```
import os
import sys

MLQD_PATH='path/to/MLQD/package'
if MLQD_PATH not in sys.path:
    sys.path.append(MLQD_PATH)

from evolution import quant_dyn
param={
```

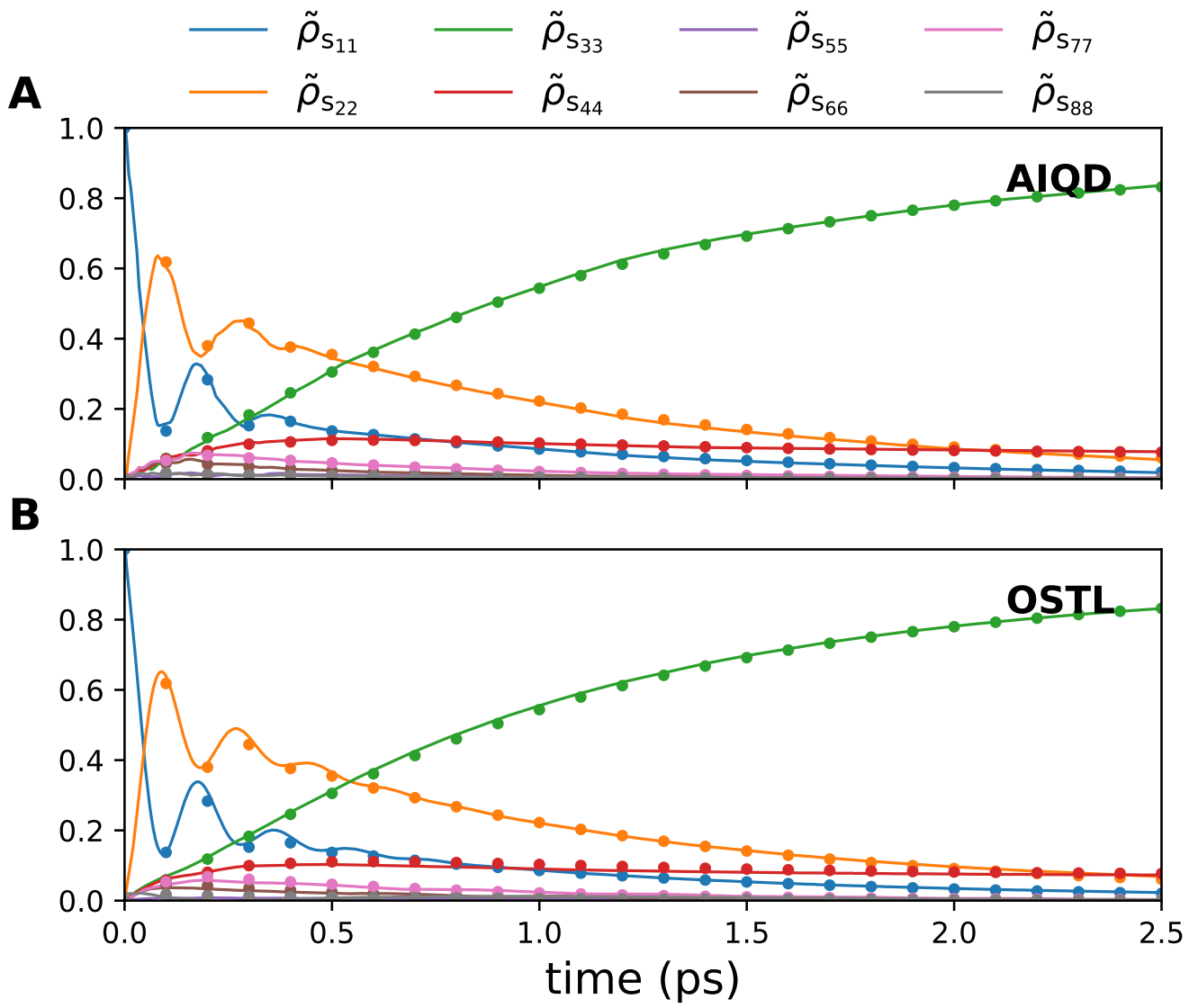

FIG. 7. The time evolution of the diagonal elements of RDM $\tilde{\rho}_s$. The initial excitation is on site 1 and other parameters are $\gamma = 125$, $\lambda = 70$, $T = 30$. The results are compared to the reference LTLME method (dots). In our calculations, γ and λ are considered in the units of cm^{-1}, while T is in the units of K.

```
        'initState': 8,
        'n_states': 8,
        'time': 50,
        'time_step': 5,
        'QDmodel': 'useQDmodel',
        'QDmodelType': 'OSTL',
        'gamma': 200.0,
        'lamb': 130.0,
        'temp': 330.0,
        'systemType': 'FMO',
        'QDmodelIn': 'OSTL_CNN_FMO_model.hdf5'
        }
quant_dyn(**param)
```

Listing 2. An example of MLQD input for predicting exciton dynamics in FMO complex using OSTL approach.

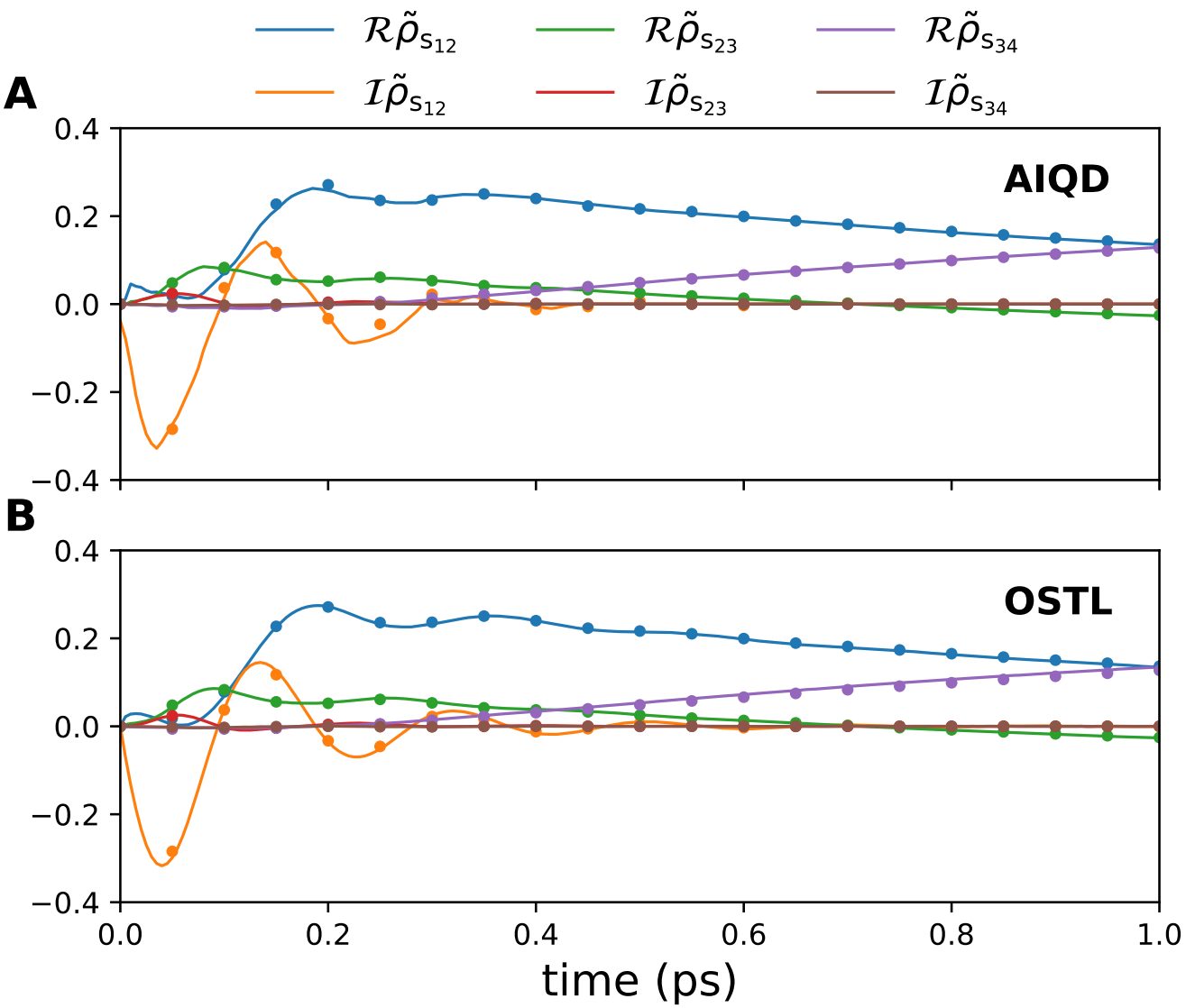

FIG. 8. The time evolution of the dominant off-diagonal terms (i.e., $\tilde{\rho}_{s_{mn}}, m \neq n$) with the initial excitation on site-1. The calligraphic R and I represent the real and imaginary parts, respectively. The results are compared to the reference LTLME method (dots). The time evolution of diagonal terms and the corresponding simulation parameters are given in Fig. 7.

IV. CONCLUSIONS

In this article, we have presented MLQD, an open-source Python package for ML-based quantum dissipative dynamics. The package provides a set of recursive (based on KRR method[91]) and non-recursive (AIQD[98] and OSTL[99]) ML approaches with the features of training an ML model, using the trained model to predict dynamics, optimization of hyperparameters and visualization of results. The package has been made available on the XACS cloud computing platform with the interface to the MLATOM package.

CODE AVAILABILITY STATEMENT

MLQD package is available on https://github.com/Arif-PhyChem/MLQD along with tutorials in Jupyter Notebooks. MLQD is also interfaced with the MLATOM@XACS package `http://mlatom.com` which allows MLQD to be used on the XACS cloud computing platform `https://xacs.xmu.edu.cn`. A user manual for MLQD on cloud computing is provided at `http:`

//mlatom.com/manual/#mlqd.

DATA AVAILABILITY STATEMENT

No data was generated in this study.

ACKNOWLEDGMENTS

We acknowledge funding by the National Natural Science Foundation of China (No. 22003051 and funding via the Outstanding Youth Scholars (Overseas, 2021) project), the Fundamental Research Funds for the Central Universities (No. 20720210092), and via the Lab project of the State Key Laboratory of Physical Chemistry of Solid Surfaces. Calculations were performed with high-performance computing resources provided by Xiamen University.

REFERENCES

[1]M. B. Plenio and S. F. Huelga, "Dephasing-assisted transport: quantum networks and biomolecules," New Journal of Physics **10**, 113019 (2008).
[2]P. Rebentrost, M. Mohseni, I. Kassal, S. Lloyd, and A. Aspuru-Guzik, "Environment-assisted quantum transport," New Journal of Physics **11**, 033003 (2009).
[3]V. May and O. Kühn, *Charge and energy transfer dynamics in molecular systems* (John Wiley & Sons, 2008).
[4]K. E. Dorfman, D. V. Voronine, S. Mukamel, and M. O. Scully, "Photosynthetic reaction center as a quantum heat engine," Proceedings of the National Academy of Sciences **110**, 2746–2751 (2013).
[5]L. Slocombe, M. Sacchi, and J. Al-Khalili, "An open quantum systems approach to proton tunnelling in dna," Communications Physics **5**, 109 (2022).
[6]F. Verstraete, M. M. Wolf, and J. Ignacio Cirac, "Quantum computation and quantum-state engineering driven by dissipation," Nature physics **5**, 633–636 (2009).
[7]W. G. Unruh, "Maintaining coherence in quantum computers," Physical Review A **51**, 992 (1995).
[8]B. Golding, M. N. Zimmerman, and S. Coppersmith, "Dissipative quantum tunneling of a single microscopic defect in a mesoscopic metal," Physical review letters **68**, 998 (1992).
[9]M. Vojta and R. Bulla, "Kondo effect of impurity moments in d-wave superconductors: Quantum phase transition and spectral properties," Physical Review B **65**, 014511 (2001).
[10]X. Wen, "Quantum field theory of many-body systems, oxford graduate texts," (2004).
[11]K. Le Hur, L. Henriet, L. Herviou, K. Plekhanov, A. Petrescu, T. Goren, M. Schiro, C. Mora, and P. P. Orth, "Driven dissipative dynamics and topology of quantum impurity systems," Comptes Rendus Physique **19**, 451–483 (2018).
[12]M. D. Reed, L. DiCarlo, S. E. Nigg, L. Sun, L. Frunzio, S. M. Girvin, and R. J. Schoelkopf, "Realization of three-qubit quantum error correction with superconducting circuits," Nature **482**, 382–385 (2012).
[13]I. Georgescu, "Trapped ion quantum computing turns 25," Nature Reviews Physics **2**, 278–278 (2020).
[14]H. Carmichael, *An open systems approach to quantum optics: lectures presented at the Université Libre de Bruxelles, October 28 to November 4, 1991*, Vol. 18 (Springer Science & Business Media, 2009).
[15]L. M. Sieberer, M. Buchhold, and S. Diehl, "Keldysh field theory for driven open quantum systems," Reports on Progress in Physics **79**, 096001 (2016).
[16]M. Milošević and R. Geurts, "The ginzburg–landau theory in application," Physica C: Superconductivity **470**, 791–795 (2010).
[17]X. Yao, "Open quantum systems for quarkonia," International Journal of Modern Physics A **36**, 2130010 (2021).
[18]Y. Wang and Y. Yan, "Quantum mechanics of open systems: Dissipaton theories," The Journal of Chemical Physics **157**, 170901 (2022).
[19]A. Jain and A. Sindhu, "Pedagogical overview of the fewest switches surface hopping method," ACS omega (2022).
[20]H.-D. Meyer and W. H. Miller, "A classical analog for electronic degrees of freedom in nonadiabatic collision processes," The Journal of Chemical Physics **70**, 3214–3223 (1979).
[21]A. G. Redfield, "On the theory of relaxation processes," IBM Journal of Research and Development **1**, 19–31 (1957).
[22]S. Nakajima, "On quantum theory of transport phenomena: steady diffusion," Progress of Theoretical Physics **20**, 948–959 (1958).
[23]R. Zwanzig, "Ensemble method in the theory of irreversibility," The Journal of Chemical Physics **33**, 1338–1341 (1960).
[24]R. Silbey and R. A. Harris, "Variational calculation of the dynamics of a two level system interacting with a bath," The Journal of chemical physics **80**, 2615–2617 (1984).
[25]A. J. Leggett, S. Chakravarty, A. T. Dorsey, M. P. Fisher, A. Garg, and W. Zwerger, "Dynamics of the dissipative two-state system," Reviews of Modern Physics **59**, 1 (1987).
[26]M. Xu, Y. Yan, Y. Liu, and Q. Shi, "Convergence of high order memory kernels in the nakajima-zwanzig generalized master equation and rate constants: Case study of the spin-boson model," The Journal of chemical physics **148**, 164101 (2018).
[27]M. Barbatti, "Nonadiabatic dynamics with trajectory surface hopping method," Wiley Interdisciplinary Reviews: Computational Molecular Science **1**, 620–633 (2011).
[28]G. Stock and M. Thoss, "Semiclassical description of nonadiabatic quantum dynamics," Physical review letters **78**, 578 (1997).
[29]J. E. Runeson and J. O. Richardson, "Spin-mapping approach for nonadiabatic molecular dynamics," The Journal of Chemical Physics **151**, 044119 (2019).
[30]J. Liu, X. He, and B. Wu, "Unified formulation of phase space mapping approaches for nonadiabatic quantum dynamics," Accounts of chemical research **54**, 4215–4228 (2021).
[31]N. Bergmann and M. Galperin, "A green's function perspective on the nonequilibrium thermodynamics of open quantum systems strongly coupled to baths: Nonequilibrium quantum thermodynamics," The European Physical Journal Special Topics **230**, 859–866 (2021).
[32]J. Cerrillo and J. Cao, "Non-markovian dynamical maps: numerical processing of open quantum trajectories," Physical review letters **112**, 110401 (2014).
[33]A. A. Kananenka, C.-Y. Hsieh, J. Cao, and E. Geva, "Accurate long-time mixed quantum-classical liouville dynamics via the transfer tensor method," The journal of physical chemistry letters **7**, 4809–4814 (2016).

[34]M. H. Beck, A. Jäckle, G. A. Worth, and H.-D. Meyer, "The multiconfiguration time-dependent hartree (mctdh) method: a highly efficient algorithm for propagating wavepackets," Physics reports **324**, 1–105 (2000).
[35]H.-D. Meyer, F. Gatti, and G. A. Worth, *Multidimensional quantum dynamics: MCTDH theory and applications* (John Wiley & Sons, 2009).
[36]B. Garraway, "Nonperturbative decay of an atomic system in a cavity," Physical Review A **55**, 2290 (1997).
[37]S. Luo, N. Lambert, and M. Cirio, "A quantum-classical decomposition of gaussian quantum environments: a stochastic pseudomode model," arXiv preprint arXiv:2301.07554 (2023).
[38]A. Nazir and G. Schaller, "The reaction coordinate mapping in quantum thermodynamics," Thermodynamics in the Quantum Regime: Fundamental Aspects and New Directions , 551–577 (2018).
[39]N. Anto-Sztrikacs and D. Segal, "Capturing non-markovian dynamics with the reaction coordinate method," Physical Review A **104**, 052617 (2021).
[40]M. Schiró and M. Fabrizio, "Real-time diagrammatic monte carlo for nonequilibrium quantum transport," Physical Review B **79**, 153302 (2009).
[41]G. Cohen and E. Rabani, "Memory effects in nonequilibrium quantum impurity models," Physical Review B **84**, 075150 (2011).
[42]F. B. Anders and A. Schiller, "Real-time dynamics in quantum-impurity systems: A time-dependent numerical renormalization-group approach," Physical review letters **95**, 196801 (2005).
[43]U. Schollwöck, "The density-matrix renormalization group," Reviews of modern physics **77**, 259 (2005).
[44]D. Xu and J. Cao, "Non-canonical distribution and non-equilibrium transport beyond weak system-bath coupling regime: A polaron transformation approach," Frontiers of Physics **11**, 1–17 (2016).
[45]A. W. Chin, Á. Rivas, S. F. Huelga, and M. B. Plenio, "Exact mapping between system-reservoir quantum models and semi-infinite discrete chains using orthogonal polynomials," Journal of Mathematical Physics **51**, 092109 (2010).
[46]J. Prior, A. W. Chin, S. F. Huelga, and M. B. Plenio, "Efficient simulation of strong system-environment interactions," Physical review letters **105**, 050404 (2010).
[47]D. E. Makarov and N. Makri, "Path integrals for dissipative systems by tensor multiplication. condensed phase quantum dynamics for arbitrarily long time," Chemical physics letters **221**, 482–491 (1994).
[48]N. Makri, "Numerical path integral techniques for long time dynamics of quantum dissipative systems," Journal of Mathematical Physics **36**, 2430–2457 (1995).
[49]N. Zhou, Y. Zhang, Z. Lü, and Y. Zhao, "Variational study of the two-impurity spin–boson model with a common ohmic bath: Ground-state phase transitions," Annalen der Physik **530**, 1800120 (2018).
[50]M. Cygorek, M. Cosacchi, A. Vagov, V. M. Axt, B. W. Lovett, J. Keeling, and E. M. Gauger, "Numerically exact open quantum systems simulations for arbitrary environments using automated compression of environments," arXiv preprint arXiv:2101.01653 (2021).
[51]Y. Tanimura and R. Kubo, "Time evolution of a quantum system in contact with a nearly gaussian-markoffian noise bath," Journal of the Physical Society of Japan **58**, 101–114 (1989).
[52]Y.-a. Yan, F. Yang, Y. Liu, and J. Shao, "Hierarchical approach based on stochastic decoupling to dissipative systems," Chemical physics letters **395**, 216–221 (2004).
[53]Y. Tanimura, "Stochastic liouville, langevin, fokker–planck, and master equation approaches to quantum dissipative systems," Journal of the Physical Society of Japan **75**, 082001 (2006).
[54]J. Jin, X. Zheng, and Y. Yan, "Exact dynamics of dissipative electronic systems and quantum transport: Hierarchical equations of motion approach," The Journal of chemical physics **128**, 234703 (2008).
[55]Q. Shi, L. Chen, G. Nan, R.-X. Xu, and Y. Yan, "Efficient hierarchical liouville space propagator to quantum dissipative dynamics," The Journal of chemical physics **130**, 084105 (2009).
[56]J. Hu, R.-X. Xu, and Y. Yan, "Communication: Padé spectrum decomposition of fermi function and bose function," (2010).
[57]J. M. Moix and J. Cao, "A hybrid stochastic hierarchy equations of motion approach to treat the low temperature dynamics of non-markovian open quantum systems," The Journal of chemical physics **139**, 134106 (2013).
[58]H. Liu, L. Zhu, S. Bai, and Q. Shi, "Reduced quantum dynamics with arbitrary bath spectral densities: Hierarchical equations of motion based on several different bath decomposition schemes," The Journal of chemical physics **140**, 134106 (2014).
[59]H. Gong, A. Ullah, L. Ye, X. Zheng, and Y. Yan, "Quantum entanglement of parallel-coupled double quantum dots: A theoretical study using the hierarchical equations of motion approach," Chinese Journal of Chemical Physics **31**, 510 (2018).
[60]L. Han, H.-D. Zhang, X. Zheng, and Y. Yan, "On the exact truncation tier of fermionic hierarchical equations of motion," The Journal of chemical physics **148**, 234108 (2018).
[61]L. Cui, H.-D. Zhang, X. Zheng, R.-X. Xu, and Y. Yan, "Highly efficient and accurate sum-over-poles expansion of fermi and bose functions at near zero temperatures: Fano spectrum decomposition scheme," The Journal of chemical physics **151**, 024110 (2019).
[62]H.-D. Zhang, L. Cui, H. Gong, R.-X. Xu, X. Zheng, and Y. Yan, "Hierarchical equations of motion method based on fano spectrum decomposition for low temperature environments," The Journal of chemical physics **152**, 064107 (2020).
[63]Z.-H. Chen, Y. Wang, X. Zheng, R.-X. Xu, and Y. Yan, "Universal time-domain prony fitting decomposition for optimized hierarchical quantum master equations," The Journal of Chemical Physics **156**, 221102 (2022).
[64]R.-X. Xu, H.-D. Zhang, X. Zheng, and Y. Yan, "Dissipaton equation of motion for system-and-bath interference dynamics," Science China Chemistry **58**, 1816–1824 (2015).
[65]W. Ying, Y. Su, Z.-H. Chen, Y. Wang, and P. Huo, "Spin relaxation dynamics with a continuous spin environment: the dissipaton equation of motion approach," arXiv preprint arXiv:2302.00215 (2023).
[66]J. T. Stockburger and H. Grabert, "Exact c-number representation of non-markovian quantum dissipation," Physical review letters **88**, 170407 (2002).
[67]W. Koch, F. Großmann, J. T. Stockburger, and J. Ankerhold, "Non-markovian dissipative semiclassical dynamics," Physical review letters **100**, 230402 (2008).
[68]J. T. Stockburger, "Exact propagation of open quantum systems in a system-reservoir context," EPL (Europhysics Letters) **115**, 40010 (2016).
[69]K. Schmitz and J. T. Stockburger, "A variance reduction technique for the stochastic liouville–von neumann equation," The European Physical Journal Special Topics **227**, 1929–1937 (2019).
[70]J. Shao, "Decoupling quantum dissipation interaction via stochastic fields," The Journal of chemical physics **120**, 5053–5056 (2004).
[71]J. Shao, "Rigorous representation and exact simulation of real gaussian stationary processes," Chemical Physics **375**, 378–379 (2010).
[72]C.-Y. Hsieh and J. Cao, "A unified stochastic formulation of dissipative quantum dynamics. ii. beyond linear response of spin baths," The Journal of chemical physics **148**, 014104 (2018).
[73]G. McCaul, C. Lorenz, and L. Kantorovich, "Partition-free approach to open quantum systems in harmonic environments: An exact stochastic liouville equation," Physical Review B **95**, 125124 (2017).
[74]Y. Ke and Y. Zhao, "Hierarchy of forward-backward stochastic schrödinger equation," The Journal of chemical physics **145**, 024101 (2016).

[75]Y. Ke and Y. Zhao, "An extension of stochastic hierarchy equations of motion for the equilibrium correlation functions," The Journal of chemical physics **146**, 214105 (2017).
[76]L. Han, V. Chernyak, Y.-A. Yan, X. Zheng, and Y. Yan, "Stochastic representation of non-markovian fermionic quantum dissipation," Physical review letters **123**, 050601 (2019).
[77]L. Han, A. Ullah, Y.-A. Yan, X. Zheng, Y. Yan, and V. Chernyak, "Stochastic equation of motion approach to fermionic dissipative dynamics. i. formalism," The Journal of Chemical Physics **152**, 204105 (2020).
[78]A. Ullah, L. Han, Y.-A. Yan, X. Zheng, Y. Yan, and V. Chernyak, "Stochastic equation of motion approach to fermionic dissipative dynamics. ii. numerical implementation," The Journal of Chemical Physics **152**, 204106 (2020).
[79]Y.-A. Yan, X. Zheng, and J. Shao, "Piecewise ensemble averaging stochastic liouville equations for simulating non-markovian quantum dynamics," New Journal of Physics **24**, 103012 (2022).
[80]J. Shao, "Dynamics of the spin-boson model at zero temperature and strong dissipation," Physical Review A **105**, 052201 (2022).
[81]O. A. von Lilienfeld, "Introducing machine learning: science and technology," Machine Learning: Science and Technology **1**, 010201 (2020).
[82]L. Zhang, A. Ullah, M. Pinheiro Jr, P. O. Dral, and M. Barbatti, "Excited-state dynamics with machine learning," in *Quantum Chemistry in the Age of Machine Learning* (Elsevier, 2023) pp. 329–353.
[83]M. Choi, D. Flam-Shepherd, T. H. Kyaw, and A. Aspuru-Guzik, "Learning quantum dynamics with latent neural ordinary differential equations," Physical Review A **105**, 042403 (2022).
[84]J. Kadupitiya, G. C. Fox, and V. Jadhao, "Solving newton's equations of motion with large timesteps using recurrent neural networks based operators," Machine Learning: Science and Technology **3**, 025002 (2022).
[85]I. Luchnikov, E. Kiktenko, M. Gavreev, H. Ouerdane, S. Filippov, and A. Fedorov, "Probing non-markovian quantum dynamics with data-driven analysis: Beyond "black-box" machine-learning models," Physical Review Research **4**, 043002 (2022).
[86]Y. Yao, C. Cao, S. Haas, M. Agarwal, D. Khanna, and M. Abram, "Emulating quantum dynamics with neural networks via knowledge distillation," arXiv preprint arXiv:2203.10200 (2022).
[87]J. Wang, Z. Chen, D. Luo, Z. Zhao, V. M. Hur, and B. K. Clark, "Spacetime neural network for high dimensional quantum dynamics," arXiv preprint arXiv:2108.02200 (2021).
[88]L. Banchi, E. Grant, A. Rocchetto, and S. Severini, "Modelling non-markovian quantum processes with recurrent neural networks," New Journal of Physics **20**, 123030 (2018).
[89]M. J. Hartmann and G. Carleo, "Neural-network approach to dissipative quantum many-body dynamics," Physical review letters **122**, 250502 (2019).
[90]F. Ge, L. Zhang, A. Ullah, and P. O. Dral, "Four-dimensional spacetime atomistic artificial intelligence models," ChemRxiv (2022).
[91]A. Ullah and P. O. Dral, "Speeding up quantum dissipative dynamics of open systems with kernel methods," New Journal of Physics (2021).
[92]L. E. H. Rodríguez, A. Ullah, K. J. R. Espinosa, P. O. Dral, and A. A. Kananenka, "A comparative study of different machine learning methods for dissipative quantum dynamics," Machine Learning: Science and Technology **3**, 045016 (2022).
[93]L. E. Herrera Rodriíguez and A. A. Kananenka, "Convolutional neural networks for long time dissipative quantum dynamics," The Journal of Physical Chemistry Letters **12**, 2476–2483 (2021).
[94]D. Wu, Z. Hu, J. Li, and X. Sun, "Forecasting nonadiabatic dynamics using hybrid convolutional neural network/long short-term memory network," The Journal of Chemical Physics **155**, 224104 (2021).
[95]K. Lin, J. Peng, C. Xu, F. L. Gu, and Z. Lan, "Automatic evolution of machine-learning based quantum dynamics with uncertainty analysis," arXiv preprint arXiv:2205.03600 (2022).
[96]S. Bandyopadhyay, Z. Huang, K. Sun, and Y. Zhao, "Applications of neural networks to the simulation of dynamics of open quantum systems," Chemical Physics **515**, 272–278 (2018).
[97]B. Yang, B. He, J. Wan, S. Kubal, and Y. Zhao, "Applications of neural networks to dynamics simulation of landau-zener transitions," Chemical Physics **528**, 110509 (2020).
[98]A. Ullah and P. O. Dral, "Predicting the future of excitation energy transfer in light-harvesting complex with artificial intelligence-based quantum dynamics," Nature communications **13**, 1–8 (2022).
[99]A. Ullah and P. O. Dral, "One-shot trajectory learning of open quantum systems dynamics," The Journal of Physical Chemistry Letters **13**, 6037–6041 (2022).
[100]F. Häse, S. Valleau, E. Pyzer-Knapp, and A. Aspuru-Guzik, "Machine learning exciton dynamics," Chemical Science **7**, 5139–5147 (2016).
[101]K. Naicker, I. Sinayskiy, and F. Petruccione, "Machine learning for excitation energy transfer dynamics," Physical Review Research **4**, 033175 (2022).
[102]F. Häse, C. Kreisbeck, and A. Aspuru-Guzik, "Machine learning for quantum dynamics: deep learning of excitation energy transfer properties," Chemical science **8**, 8419–8426 (2017).
[103]A. Farahvash, C.-K. Lee, Q. Sun, L. Shi, and A. P. Willard, "Machine learning frenkel hamiltonian parameters to accelerate simulations of exciton dynamics," The Journal of Chemical Physics **153**, 074111 (2020).
[104]M. Secor, A. V. Soudackov, and S. Hammes-Schiffer, "Artificial neural networks as propagators in quantum dynamics," The Journal of Physical Chemistry Letters **12**, 10654–10662 (2021).
[105]A. V. Akimov, "Extending the time scales of nonadiabatic molecular dynamics via machine learning in the time domain," The Journal of Physical Chemistry Letters **12**, 12119–12128 (2021).
[106]K. Lin, J. Peng, C. Xu, F. L. Gu, and Z. Lan, "Realization of the trajectory propagation in the mm-sqc dynamics by using machine learning," arXiv preprint arXiv:2207.05556 (2022).
[107]D. Tang, L. Jia, L. Shen, and W.-H. Fang, "Fewest-switches surface hopping with long short-term memory networks," The Journal of Physical Chemistry Letters **13**, 10377–10387 (2022).
[108]P. O. Dral, "Mlatom: A program package for quantum chemical research assisted by machine learning," Journal of computational chemistry **40**, 2339–2347 (2019).
[109]P. O. Dral, F. Ge, B.-X. Xue, Y.-F. Hou, M. Pinheiro, J. Huang, and M. Barbatti, "Mlatom 2: An integrative platform for atomistic machine learning," Topics in Current Chemistry **379**, 1–41 (2021).
[110]P. O. Dral, P. Zheng, B.-X. Xue, F. Ge, Y.-F. Hou, J. Max Pinheiro, Y. Su, Y. Dai, and Y. Chen, *MLatom: a Package for Atomistic Simulations with Machine Learning. http://mlatom.com (accessed on Feb 13, 2023)*, Xiamen University, Xiamen, China (2013–2023).
[111]J. Bergstra, R. Bardenet, Y. Bengio, and B. Kégl, "Algorithms for hyper-parameter optimization," Advances in neural information processing systems **24** (2011).
[112]J. Bergstra, B. Komer, C. Eliasmith, D. L. K. Yamins, and D. D. Cox, "Hyperopt: a python library for model selection and hyperparameter optimization," Computational Science & Discovery **8**, 014008 (2015).
[113]X. University, *XACS: Xiamen Atomistic Computing Suite. http://XACScloud.com (accessed on Feb 16, 2023)*, Xiamen University, Xiamen, China (2022–2023).

[114]A. Ullah, L. E. H. Rodríguez, P. O. Dral, and A. A. Kananenka, "Qd3set-1: A database with quantum dissipative dynamics data sets," arXiv preprint arXiv:0000000 (2023).
[115]F. Stulp and O. Sigaud, "Many regression algorithms, one unified model: A review," Neural Networks **69**, 60–79 (2015).
[116]P. O. Dral, "Quantum chemistry assisted by machine learning," in *Advances in Quantum Chemistry*, Vol. 81, edited by K. Ruud and E. J. Brändas (Elsevier, 2020) pp. 291–324.
[117]C. E. Rasmussen, "Gaussian processes in machine learning," in *Advanced Lectures on Machine Learning: ML Summer Schools 2003, Canberra, Australia, February 2 - 14, 2003, Tübingen, Germany, August 4 - 16, 2003, Revised Lectures* (Springer Berlin Heidelberg, Berlin, Heidelberg, 2004) pp. 63–71.
[118]T. Gneiting, W. Kleiber, and M. Schlather, "Matérn cross-covariance functions for multivariate random fields," Journal of the American Statistical Association **105**, 1167–1177 (2010).
[119]K. Hornik, M. Stinchcombe, and H. White, "Multilayer feedforward networks are universal approximators," Neural Netw. **2**, 359–366 (1989).
[120]G. Cybenko, "Approximation by superpositions of a sigmoidal function," Math. Control Signals Syst. **2**, 303–314 (1989).
[121]M. Leshno, V. Y. Lin, A. Pinkus, and S. Schocken, "Multilayer feedforward networks with a nonpolynomial activation function can approximate any function," Neural Netw. **6**, 861–867 (1993).
[122]A. O. Caldeira and A. J. Leggett, "Path integral approach to quantum brownian motion," Physica A: Statistical mechanics and its Applications **121**, 587–616 (1983).
[123]J. R. Johansson, P. D. Nation, and F. Nori, "Qutip: An open-source python framework for the dynamics of open quantum systems," Computer Physics Communications **183**, 1760–1772 (2012).
[124]A. Ishizaki and G. R. Fleming, "Unified treatment of quantum coherent and incoherent hopping dynamics in electronic energy transfer: Reduced hierarchy equation approach," The Journal of chemical physics **130**, 234111 (2009).
[125]M. Schmidt am Busch, F. Muh, M. El-Amine Madjet, and T. Renger, "The eighth bacteriochlorophyll completes the excitation energy funnel in the fmo protein," The journal of physical chemistry letters **2**, 93–98 (2011).
[126]C. Olbrich, T. L. Jansen, J. Liebers, M. Aghtar, J. Strümpfer, K. Schulten, J. Knoester, and U. Kleinekathöfer, "From atomistic modeling to excitation transfer and two-dimensional spectra of the fmo light-harvesting complex," The Journal of Physical Chemistry B **115**, 8609–8621 (2011).
[127]S. Bourne Worster, C. Stross, F. M. Vaughan, N. Linden, and F. R. Manby, "Structure and efficiency in bacterial photosynthetic light harvesting," The Journal of Physical Chemistry Letters **10**, 7383–7390 (2019).
[128]J. W. Abbott, "Quantum dynamics of bath influenced excitonic energy transfer in photosynthetic pigment-protein complexes," Master Thesis, University of Bristol United Kingdom https://doi.org/10.5281/zenodo.7229807 (2020).
[129]J. W. Abbott, "jwa7/quantum_heom," Github repository: https://github.com/jwa7/quantum_HEOM, (accessed on Feb 13, 2023) (2019).